Influence of 4-Guanidinobutyric Acid as Coadsorbent in Reducing Recombination in Dye-Sensitized Solar Cells

Zhipan Zhang,[†] Shaik M. Zakeeruddin,[†] Brian C. O'Regan,[‡] Robin Humphry-Baker,[†] and Michael Grätzel*,[†]

Laboratory for Photonics and Interfaces, Institute of Chemical Sciences and Engineering, Swiss Federal Institute of Technology, CH-1015 Lausanne, Switzerland, and Electronic Materials and Devices, Department of Chemistry and Physics, Imperial College, SW7 2AZ London, United Kingdom

Received: August 3, 2005; In Final Form: September 20, 2005

Dye-sensitized solar cells based on nanocrystalline TiO_2 have been fabricated with an amphiphilic ruthenium sensitizer [Ru (4,4′-dicarboxylic acid-2,2′-bipyridine) (4,4′-bis(p-hexyloxystyryl)-2,2′-bipyridine)$(NCS)_2$], coded as K-19, and 4-guanidinobutyric acid (GBA) as coadsorbent. The cells showed a ∼50 mV increase in open-circuit voltage and a similar current in comparison with cells without GBA cografting. The performance of both types of devices was evaluated on the basis of their photocurrent−voltage characteristics, dark current measurements, cyclic voltammetry, electrochemical impedance spectroscopy, and phototransient decay methods. The results indicate that GBA shifted the conduction band of TiO_2 toward a more negative potential and reduced the interfacial charge-transfer reaction from conduction band electrons to triiodide in the electrolyte (also known as the back reaction). In addition, the devices with GBA cografting showed an excellent stability with a power conversion efficiency of approximately 8% under simulated full sunlight (air mass 1.5, 100 mW cm^{-2}) during visible light soaking at 60 °C.

Introduction

The success of dye-sensitized solar cells (DSCs) has increasingly fostered scientific and industrial research on the photovoltaic properties of wide band gap oxides, mainly TiO_2-based, solar cells during the past years.[1−3] Unlike conventional p−n junction solar devices, a DSC employs interconnected inorganic semiconductor nanocrystals to form a "bulk" junction with a huge surface area at the semiconductor/electrolyte interface and, thus, provides sufficient anchoring sites for sensitizers to attain effective light harvesting and energy conversion. Achieving more than 11% efficiency with acetonitrile-based electrolyte and 8% long-term stability at 80 °C with a low volatile electrolyte have transformed DSC into a more attractive candidate as a substitute for conventional silicon solar cells.[4−6]

However, the ideal of a "bulk" junction is impaired by the occurrence of interfacial charge recombination of photoinjected electrons, the main processes being depicted in Scheme 1. Under illumination, the sensitizer is excited and injects electrons into the conduction band (CB) of the mesoscopic TiO_2 film. Electron transfer from a donor, most typically the iodide, then regenerates the dye ground state. The transportation of the electrons in TiO_2 is strongly influenced by trapping (1) and detrapping (2) effects. Previous results showed that trapping is about 3 orders faster than detrapping, so nearly all photoinjected electrons are located in trap states.[7,8] The source of recombination includes the recapture of injected electrons in these traps by the oxidized sensitizer (S^+) anchored on the TiO_2 surface (3) or back reaction with the oxidized component of the redox couple present in the electrolyte, I_3^- (4). Considering the relatively fast regeneration of dye by iodide, the latter would be expected to be the predominant recombination channel in DSCs. Apart from the very large area of the junction, the recombination is favored by the fact that the size of the nanoparticles is too small to support enough band bending, which would generate an internal electric field that is believed to be essential to afford charge separation in photoelectrochemical devices.[3] Theoretically, the back reaction can be blocked by surface modifications, such as introducing an insulating layer on the solvent-exposed parts of the nanoporous electrode in order to passivate the interface[9,10] or when core−shell structured particles were used instead of bare TiO_2.[11−14] Coating of TiO_2 nanoparticles with a shell material of a slightly more negative CB will result in an energy barrier that assists electron injection while retarding its diffusion in the opposite direction. In both of these cases, the devices showed

SCHEME 1: Schematic Diagram Showing Electron Transportation and Recombination Processes in a Dye-Sensitized Nanocrystalline Solar Cell with a Liquid-based I_3^-/I^- Electrolyte[a]

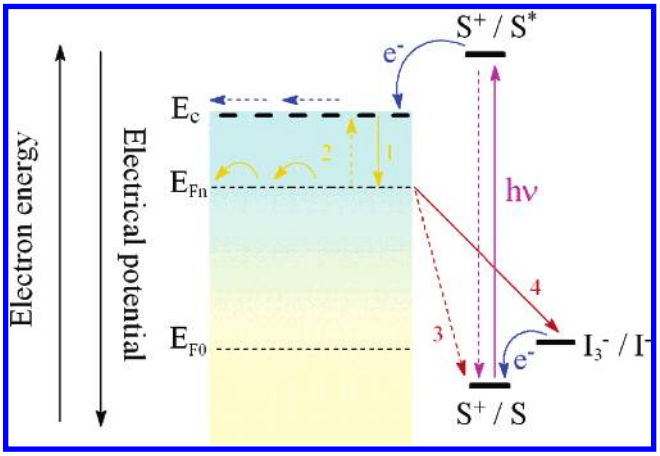

[a] Trapping (1) and detrapping (2) of electrons in TiO_2. Recombination of trapped electrons with the oxidized sensitizer S^+ (3) and with the redox couple (4).

* Corresponding author. E-mail address: michael.graetzel@epfl.ch.
† Swiss Federal Institute of Technology.
‡ Imperial College.

10.1021/jp054305h CCC: $30.25
Published on Web 10/29/2005

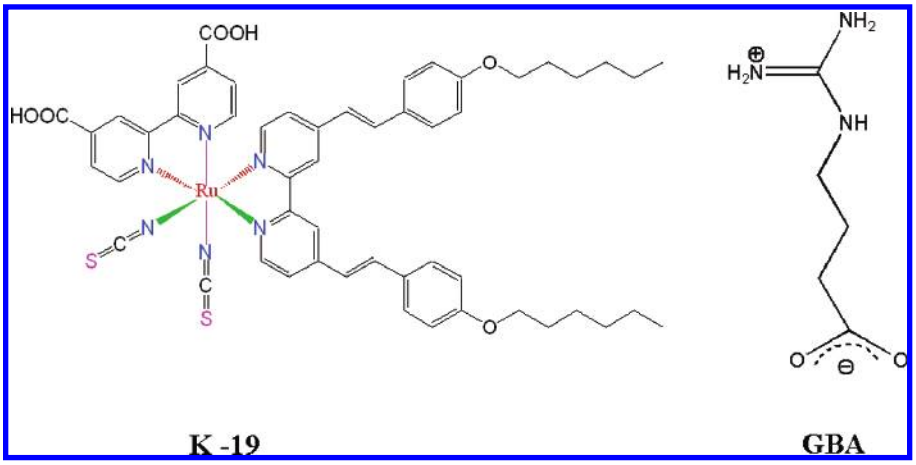

Figure 1. Structure of the K-19 sensitizer and GBA

higher values of short-circuit current density (J_{sc}), open-circuit voltage (V_{oc}) and fill factor (*FF*), and thus, better performance.

Cografting of dyes with amphiphilic molecules containing carboxylic or phosphonic end groups were reported to considerably enhance the stability and the performance of DSCs.[6,15−17] The coadsorption leads to the formation of a more compact monolayer, comprised of the dye and coadsorbent, than the adsorption of dye alone. This insulating molecular layer effectively shields the back electron transfer from the TiO_2 conduction band to triiodide and gives a higher open-circuit voltage. In this paper, an amphiphilic ruthenium sensitizer coded as K-19 is coadsorbed with 4-guanidinobutyric acid (GBA), a combination that enhances the open-circuit voltage by 50 mV and increases the overall conversion efficiency by 10%. Photovoltage transient measurements and electrochemical impedance spectroscopy techniques were applied in order to understand the role of the coadsorbent in the enhancement of the efficiency and open-circuit potential. The results have shown that the presence of the coadsorbent resulted in a small negative shift of the conduction band edge of TiO_2 nanocrystals as well as a decrease in the back reaction rate constant.

Experimental Section

Reagents and Electrolytes. All chemicals and solvents used in the present work were of puriss quality. *N*-methylbenzimidazole (NMBI) was purchased from Aldrich and recrystallized from diethyl ether before use. GBA was purchased from Fluka and used as obtained. 3-Methoxypropionitrile (MPN) puriss quality was obtained from Fluka and distilled before use. K-19 was synthesized as reported in our earlier publication,[17] and the structure is shown in Figure 1. 1-Methyl-3-propylimidazolium iodide (PMII) was prepared according to the literature method[15] and its purity confirmed by ^{1}H NMR spectrum. Sephadex LH-20 was obtained from Pharmacia (Sweden). TiO_2 particles of 400 nm size were received as a gift from CCIC (Japan). The electrolyte contained 0.8 M 1-propyl-3-methylimidazolium iodide, 0.15 M I_2, 0.1 M guanidinium thiocyanate, and 0.5 M *N*-methylbenzimidazole in MPN.

Spectroscopic Measurements. IR spectra were measured by using a FTS 7000 FTIR spectrometer (Digilab, USA). Spectra were derived from 64 scans at a resolution of 2 cm^{-1}. All samples were measured under identical mechanical force used to push the mesoscopic TiO_2 films in contact with the diamond window. No ATR correction has been applied to the data. The dye-loaded electrodes were rinsed in acetonitrile and dried prior to measuring the spectra.

For photoelectrochemical measurements, a 450 W xenon light source (Oriel, USA) was used to give an irradiance of 100 mW cm^{-2} (the equivalent of one sun at AM 1.5) at the surface of the solar cell. The spectral output of the lamp was matched in the region of 350−750 nm with the aid of a Schott K113 Tempax sunlight filter (Präzisions Glas & Optik GmbH, Germany) so as to reduce the mismatch between the simulated and true solar spectra to less than 2%. Various incident light intensities were regulated with neutral wire mesh attenuators. The current voltage characteristics of the cell under these conditions were obtained by applying an external potential bias to the cell and measuring the generated photocurrent with a Keithley model 2400 digital source meter (Keithley, USA).

Photovoltage transients were observed by using a pump pulse generated by a ring of red LEDs controlled by a fast solid-state switch. Pulse widths of 100 μs were used, with a rise and fall time of $\leq$2 μs. The pulse was incident on the photoanode side of the cell, and its intensity was controlled to keep the modulation of the voltage below 10 mV. White bias light, also incident on the same side of the cell, was supplied by 10 W "Solarc" lamps (WelchAllyn) that are also of the metal−halogen type. The bias light was attenuated when needed by neutral-density filters. When the pulse intensity from the red diodes was insufficient to give voltage signals greater than 0.5 mV, a white flash lamp was used. The flash time was also 100 μs, with a fall half time of 20 μs. The time resolution of the potentiostat is 20 μs; thus, transient phenomena with time constants $\geq$40 μs could be measured. It is important to note the Solarc light sources contain a UV component similar to that found in sunlight.

Cyclic voltammetry measurements were performed on a computer-controlled Autolab P20 electrochemical workstation (Eco Chimie, Netherlands) in combination with a conventional three-electrode, one-compartment electrochemical cell. A dye-coated nanocrystalline TiO_2 film in the absence (electrode A) or presence (electrode B) of GBA cografting was employed as the working electrode. A Pt foil and an Ag disk were used as counter and reference electrodes, respectively. The reference electrode was calibrated by measuring the redox potential of ferrocene dissolved in 1-methyl-3-ethylimidazolium bis (trifluoromethyl) sulfonyl) imide (EMITFSI), and the redox potentials were converted to those vs a normal hydrogen electrode (NHE) reference scale by adding a constant of 0.67 V.

Impedance measurements were performed with a computer-controlled potentiostat (EG&G, model 273) equipped with a frequency response analyzer (EG&G, model 1025). The frequency range is 0.005−100 kHz, and the magnitude of the

modulation signal is 10 mV. The obtained spectra were fitted with Z-View software (v2.1b, Scribner Associates Inc.) in terms of appropriate equivalent circuits.

Device Fabrication. A double-layer TiO_2 mesoscopic film was used as the photoanode. An 8-μm-thick transparent layer of 20-nm-sized TiO_2 particles was first printed on the fluorine-doped SnO_2 conducting glass electrode and further coated with a 5-μm-thick second layer of 400 nm light-scattering anatase particles. The details for the preparation of mesoscopic TiO_2 film has been described elsewhere.[16,18] The double-layer structured TiO_2 electrode was first sintered at 500 °C for 20 min and cooled at ambient temperature down to 80 °C. It was then immersed into the dye solution at room temperature for 12 h before assembly with a thermally platinized conducting glass counter electrode. For the present work, two kinds of sensitizer solution were used. Solution A consisted of 0.3 mM K-19 dye in acetonitrile and *tert*-butyl alcohol (volume ratio, 1:1), while solution B contained 0.3 mM K-19 dye and 0.3 mM GBA as coadsorbent in the same solvent. To prepare solution B, GBA was first dissolved in 10% water and ethanol mixture (30 mM) then added to the dye solution to bring it to 0.3 mM GBA. The electrodes were separated by a 35-μm-thick Bynel hot-melt ring (DuPont, USA) and sealed by heating. The internal space was evacuated, then filled with electrolyte through a filling hole made by a sandblasting drill on the counter electrode glass substrate. Finally, the electrolyte introduction hole was sealed with a Bynel sheet under a thin glass cover by heating to produce device A without and device B with GBA cografting.

Stability Test. Hermetically sealed cells were used for long-term stability tests under moderate thermal stress and visible light soaking. After a short thermal aging in the oven, the cells were covered with a 50-μm-thick polyester film (Preservation Equipment Ltd, UK) as a UV cutoff filter (below 400 nm) and irradiated at open circuit under a Suntest CPS plus lamp (ATLAS GmbH, 100 mW cm^{-2}, 60 °C).

Analysis. Electrochemical impedance spectroscopy (EIS) is a well-known technique for characterization of electrochemical systems. As a steady-state method, it modulates the external voltage bias and measures the synchronized response as a function of frequency. Recently, several groups have reported interesting results by using EIS to evaluate the performance of DSCs, including our own publication.[19−28] In principle, the modulation of external voltage results in a fluctuation of the quasi-Fermi level of the TiO_2 electrode, which changes (i) the population of surface and bulk states with electrons and (ii) the recombination current across the TiO_2/electrolyte interface. Hence, analyzing EIS measured in the dark with an appropriate model proposed by Bisquert[24] yields parameters of chemical capacitance C_μ and charge-transfer resistance R_{rec}, corresponding to effect (i) and (ii), respectively. In the present work, the EIS spectra of the cell were measured at forward biases near its V_{oc}, C_μ is taken as the TiO_2 film capacitance, which is proportional to the density of states (DOS), including both surface and bulk traps. R_{rec} reflects the direct transfer of electrons from the oxide conduction band to the triiodide in the electrolyte. The product of these two quantities gives a time constant, the observed electron lifetime, $\tau_r = R_{rec}C_\mu$. This τ_r relates more properly to the *response time* with a general meaning of the characteristic time for the decay under a small perturbation,[25] yet it is often interpreted as the *electron lifetime* and we used the latter term in our discussion.

In transient photovoltage experiments, we used red diodes as a probe to generate a perturbation near the V_{oc} of the cell under the bias light and measured the voltage decay process thereafter. Normally, the decay follows closely a single exponential form, thus the recombination rate constant, k, can be extracted from the slope of the semilogarithmic plot. The capacitance of the TiO_2/electrolyte interface and DOS at the V_{oc} are calculated as $C = \Delta Q/\Delta V$, where ΔV is the peak of the transient, and ΔQ is the number of electrons injected during the light flash. The latter is determined by integrating a photocurrent transient at short circuit condition generated from an identical pulse. This method may underestimate the actual injected charge by the fraction of electrons that are lost to recombination during transport. The error is thought to be less than 30% in the worst case, and more critically, it will affect only the magnitude but not the shape of the calculated capacitance vs potential curves.[29,30]

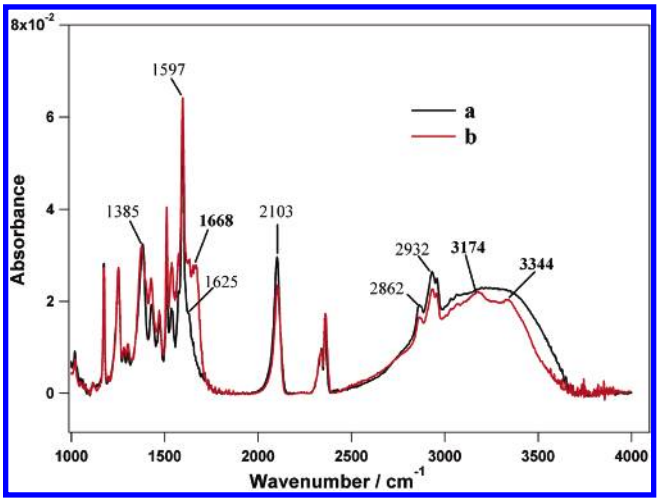

Figure 2. ATR−FTIR spectra for TiO_2 films stained with (a) K-19 dye alone and (b) K-19 dye and GBA.

Results and Discussion

Figure 2 shows the attenuated total reflectance FTIR (ATR-FTIR) spectra of nanoporous TiO_2 electrode A and electrode B with typical peaks of K-19 sensitizer as we have reported before.[17] The single feature at 2103 cm^{-1} arises from the thiocyanato group, the bands at 1625 cm^{-1} and 1385 cm^{-1} are for the asymmetric and symmetric stretching modes of carboxylate groups, and the signals observed at 2932 and 2862 cm^{-1} correspond to the asymmetric and symmetric stretching modes of the CH_2 units. The sharp absorption at 1597 cm^{-1} is attributed to the vibration mode of the double bond between two aromatic rings. The peaks located at 1538 and 1429 cm^{-1} are ascribed to the aromatic modes of bipyridyl, while the broad band centered at 3440 cm^{-1} is due to adsorbed water, presumably from the dye solution because the TiO_2 film is heated prior to staining.

Spectrum b was measured with electrode B, which was stained from the solution consisting of K-19 sensitizer and GBA at equal concentrations. It is well established that the characteristic peak of the thiocyanato group at 2103 cm^{-1} is a sensitive measure of the adsorbed amount of sensitizer.[6] The fact that the intensity of this peak for K-19 showed a decrease by about 25% indicates that $^1/_4$ of the dye has been replaced by GBA during coadsorption. The decrease in the concentration of dye on the surface of the TiO_2 electrode is also confirmed by measuring the transparent films by UV−vis spectroscopy. Because of the presence of GBA on electrode B, several new bands are observed. The peak at ca. 1668 cm^{-1} is due to the asymmetric stretching of the carboxylate group of GBA. In comparison with its counterpart resulting from the pure K-19

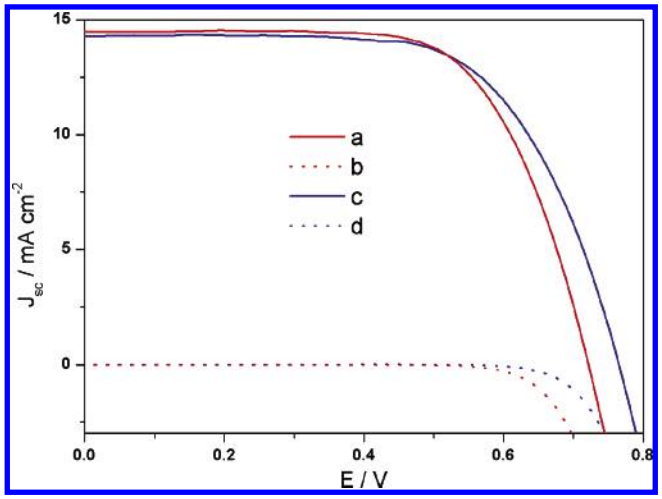

Figure 3. Current density−voltage characteristics of (a) device A and (c) device B under AM 1.5 simulated sunlight (100 mW cm^{-2}) illumination. Dark current data for device A and device B are shown as curves (b) and (d), respectively.

TABLE 1: Current/Voltage Parameters of DSCs (Device A and Device B)

	η (%) at different light intensities[a]			current/voltage characteristics at 1.0 sun		
device	0.1 sun	0.5 sun	1.0 sun	V_{oc} (mV)	J_{sc} (mA cm^{-2})	FF
A	7.9	7.6	6.9	719	14.5	0.671
B	8.7	8.4	7.5	767	14.3	0.682

[a] The spectral distribution of the xenon lamp simulates air mass 1.5 solar light. 1.0 sun corresponds to ~100 mW cm^{-2}. The cell active areas were 0.158 cm^{-2}.

sensitizer, the carboxylate group of GBA does not exhibit conjugation with the pyridine ring, and consequently, the absorption appears at higher wavenumbers. Likewise, two conspicuous peaks centered at 3174 and 3344 cm^{-1} correspond to the N−H stretching modes of the guanidino group. These spectroscopic data are convincing evidence that a mixed layer of K-19 and GBA has been cografted onto electrode B.

Figure 3 shows the corresponding photocurrent density vs voltage curves of device A and device B at full sun illumination and in the dark. The parameters of short-circuit current density (J_{sc}), open-circuit voltage (V_{oc}), fill factor (*FF*) for both cells, and photovoltaic conversion efficiency (η) are listed in Table 1. Compared with device A, device B has similar current and fill factor, but a higher open-circuit voltage, making device B superior to device A. This result is further corroborated by measurements at different light intensities. Using GBA as coadsorbent enhances the overall power conversion efficiency due to an increase in the open-circuit voltage of the device without significant penalty in photocurrent.

The dark current is not a good simulation of the recombination current under illumination due to the localized variation in electrolyte concentration and potential distribution through the TiO_2 electrode. However, it can be used as an estimate of the extent of reduction of triiodide with conduction band electrons. The dark current data in Figure 3 suggest that the mixed monolayer of K-19 and GBA is more effective in retarding this back reaction, a finding consistent with the ~50 mV increase in $V_{oc.}$ Because V_{oc} is determined by the difference between the quasi-Fermi level and the redox potential of triiodide/iodide couple in the electrolyte, a higher V_{oc} implies a negative shift of the quasi-Fermi level of TiO_2 induced by GBA coadsorbent.

Cyclic voltammograms of electrode A and electrode B were measured in the ionic liquid EMITFSI. The choice of EMITFSI as the electrolyte for these studies is based upon the insolubility of K-19 sensitizer in this medium, thus avoiding any dye desorption from the TiO_2 electrode over the entire potential range investigated during the electrochemical measurement. Applying an increasing negative potential, i.e., a forward bias, on the TiO_2 layer in the EMITFSI ionic liquid moved the quasi-Fermi level closer toward its conduction band and led to a capacitive current as shown in Figure 4a. In principle, for a perfect n-type semiconductor−electrolyte junction, charge injection will commence once the quasi-Fermi level reaches the lower edge of the conduction band. However, because of the presence of coordinatively unsaturated Ti species on the surface of TiO_2 nanoparticles, some electronic levels exist at energies below the conduction band edge.[3,31] These surface states trap electrons injected under forward bias, producing a gradual onset of the capacitive current in the forward scan as shown in Figure 4a.

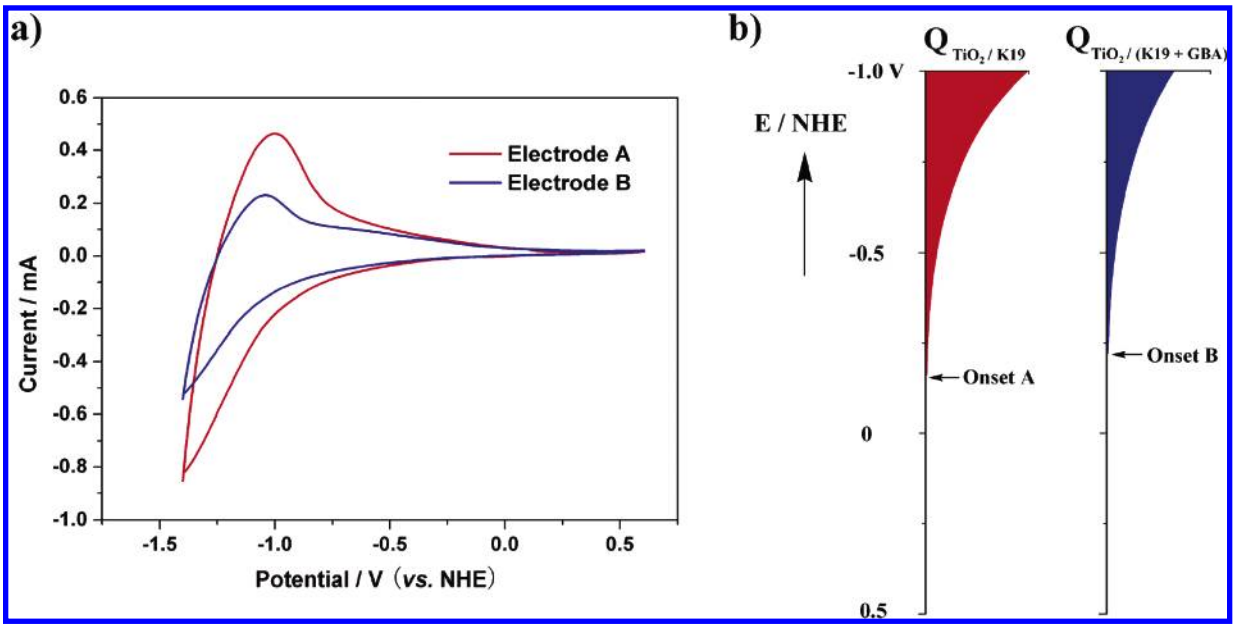

Figure 4. (a) Cyclic voltammograms of TiO_2 electrode A (K-19 grafted only) and electrode B (GBA cografted) in EMITFSI. Straight red line for Electrode A, coated with K-19 sensitizer alone; blue line for Electrode B, K-19/GBA cografted. The scan rate is 0.05 V/s. (b) Energy levels at the mesoscopic TiO_2/EMITFSI interface.

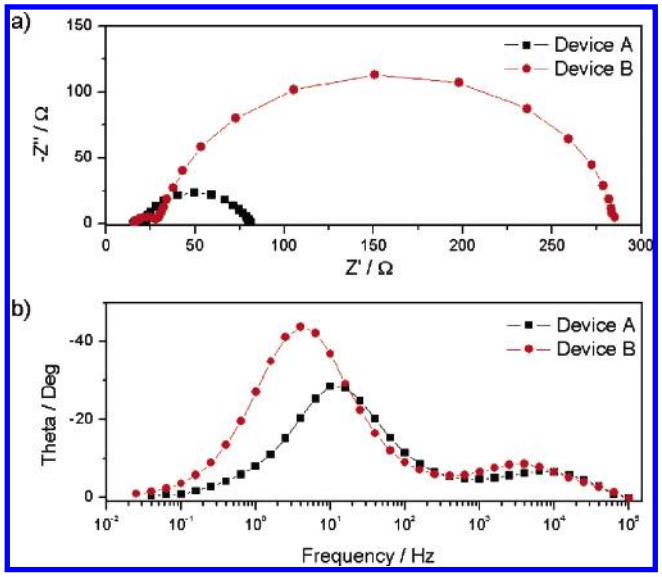

Figure 5. Typical electrochemical impedance spectra of device A and B in the forms of (a) Nyquist plots and (b) Bode plots. The spectra were measured with an external potential of −0.72 V in the dark.

For the reverse scans, the current approached zero at the more positive potentials, indicating recovery of the injected negative charge and regeneration of most surface states.[32]

The energetic distribution of the traps at the surface of a TiO_2 electrode can be deduced from the cyclic voltammograms via the following equations

$$\frac{dQ}{dV} = \mathrm{DOS}\frac{N_A}{F} \quad (1)$$

$$dQ = \frac{1}{\upsilon} I(V)dV \quad (2)$$

where Q is the total injected charge, N_A is the Avogadro constant, F is Faraday's constant, $I(V)$ is the current, V is the potential applied on the electrode, and υ represents the constant scanning rate in the cyclic voltammetry measurements. Dividing the derivative dQ/dV by the elementary charge in eq 1 yields DOS, while the integration of eq 2 will give Q the total number of surface states as plotted vs applied potential in Figure 4b. The onset is around −0.15 V (vs NHE) for electrode A, whereas in the case of electrode B, it moves to −0.20 V (vs NHE), indicating that the edge of conduction band of TiO_2 moved negatively toward the vacuum level. Because there is not a steep gradient, Q for electrode B increases much more slowly than Q for electrode A under increasing forward bias. This phenomenon is due to better surface passivation. TiO_2 nanocrystals are not fully covered by the dye molecules, and consequently, there are some surface areas directly in contact with the electrolyte. The use of GBA as coadsorbent passivates these surface areas, resulting in a decrease in trap states.

Figure 5 shows typical electrochemical impedance spectra of device A and B measured in the dark. The figure is presented in the forms of (a) Nyquist plots and (b) Bode plots. For clarity of comparison, an identical forward bias of −0.72 V, which is the V_{oc} of device A, was applied to both cells. In Figure 5a, the Nyquist plots consist of two semicircles. The smaller semicircle occurring at higher frequencies represents redox charge transfer at the platinum counter electrode, while the larger one at lower frequencies is attributed to the electron transport in the TiO_2 layer, the electron transfer at the oxide/electrolyte interface and ion diffusion within the electrolyte. Fitting the low-frequency semicircle subsequently gives C_μ and R_{rec}. Comparing device B with device A, C_μ decreased from 2600 to 2000 μF cm^{-2} (in terms of cell area), while R_{rec} increased sharply from 54.8 to 254.7 Ω, yielding a larger τ_r of 127.6 ms for device B than that for device A, i.e., 35.6 ms. These results are supported by the Bode plots shown in Figure 5b. Here, the frequency value of the phase angle peak approximately equals the reciprocal of τ_r. Following this principle, the τ_r extracted for device A and device B are ∼50 and ∼200 ms, respectively, in fair agreement with the results from the Nyquist plots.

To elucidate the underlying mechanisms connected to these differences, impedance spectra were also measured by varying the applied potential at equal intervals in the vicinity of V_{oc}. The values of C_μ, R_{rec}, and τ_r are plotted in Figure 6. C_μ follows a characteristic exponential rise with increasing forward bias. This behavior is generally analyzed to yield the chemical capacitance of nanostructured TiO_2 by using the following model [20,33,34]

$$C = C_a \exp[-\alpha eV/k_B T] + C_b \quad (3)$$

where k_B is the Boltzmann constant, T is the temperature, e is the elementary charge, V is the applied potential, C_a is the prefactor of the exponential increase, C_b is the quasiconstant capacitance at low potentials, and α is a coefficient describing either the Boltzmann occupancy of the conduction band capacitance ($\alpha = 1$) or an exponential distribution of trap states ($\alpha < 1$). We found α of 0.24 for device A and 0.17 for device B, respectively, results very similar to those reported in previous work yielding α values of 0.2−0.3.[27,33]

The plot of electron lifetime (response time) vs bias potential is shown in Figure 6d. It is interesting that device B has a much longer response time than device A at any given potential. This increase in τ_r is associated with a pronounced rise in the charge-transfer resistance, indicating that the cografting of GBA decreases the interfacial rate constant for electron capture by triiodide ions. GBA assists probably the self-assembly of the K-19 dye at the TiO_2 surface, producing a more compact monolayer than when the sensitizer is adsorbed alone that blocks the access of I_3^- to the interface impairing the back reaction.

GBA also lowers the film capacitance, C_μ, due to the passivation of surface states and induces a negative band edge movement, reducing the number of recombination centers available at a given cell potential. Both effects augment the quasi-Fermi level of the conduction band electrons in the titania film and increase, therefore, the open-circuit photovoltage of the solar cell.

The treatment of the titania surface with agents such as with 4-*tert*-butylpyridine or ammonia also produces an increase in open-circuit voltage. However, a significant drop in photocurrent generally accompanies this effect.[35] The main role of such additives is to depronotate the TiO_2 surface, synchronously displacing the quasi-Fermi energy and conduction band edge toward the vacuum level. This negative shift of the conduction band hampers electron injection from the excited sensitizer, explaining the decrease in the photocurrent. While such a shift occurs also with GBA as coadsorbent, it is small enough not to affect the electron injection from the excited sensitizer into the conduction band of titania. The main effect of GBA is to block the electron recapture by the redox electrolyte, allowing higher electron concentrations in the mesoscopic TiO_2 films and hence a higher V_{oc} to be reached under illumination.

Finally, it should be noted that GBA has a significant dipole moment, which can alter the energetics of the TiO_2/sensitizer interface unless it is locally compensated by solvent molecules.

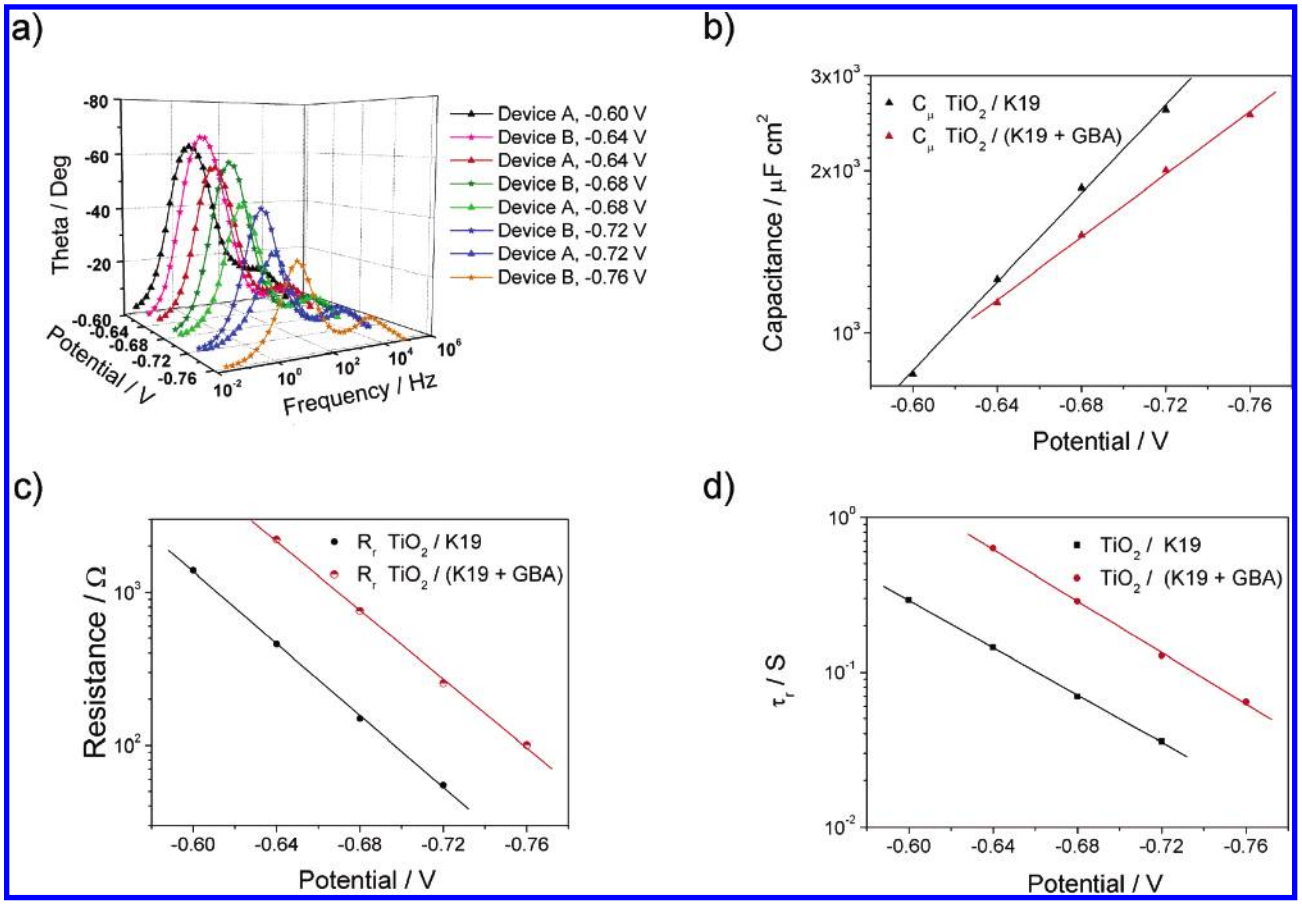

Figure 6. (a) Electrochemical impedance spectra of device A (TiO_2 electrode coated with K-19 dye alone) and device B (TiO_2 film stained with K-19 and GBA) measured at different forward bias near their open-circuit potentials. The fitted results are plotted as (b) film capacitance C_μ, (c) charge-transfer resistance R_{rec}, and (d) electron lifetime τ_r with respect to the externally controlled potential.

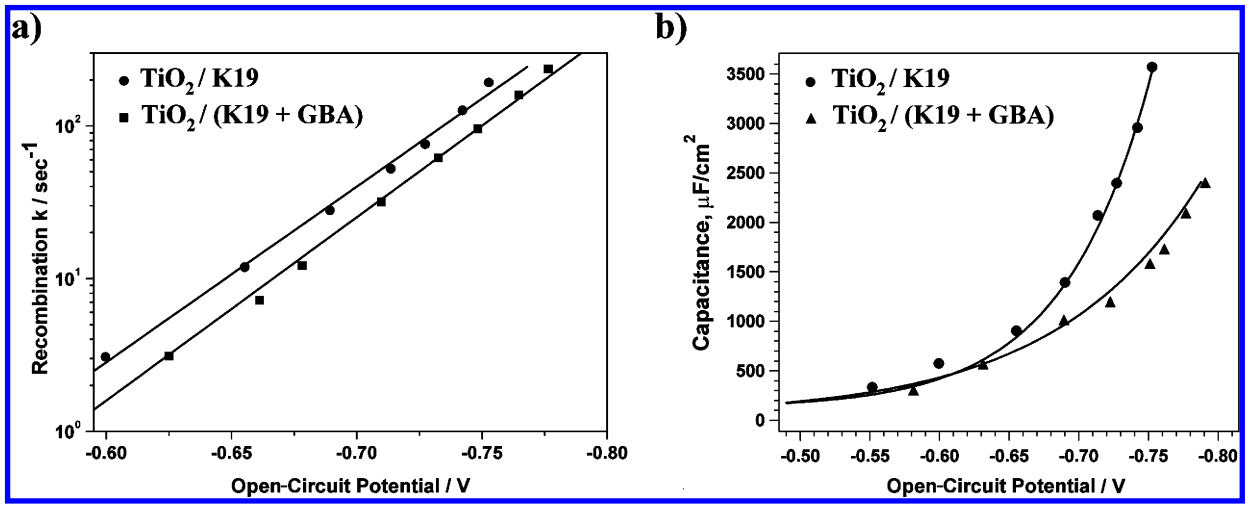

Figure 7. Results of phototransient voltage measurements with cells made by nanoporous TiO_2 films in the absence and presence of GBA cografting. (a) Recombination rate constant vs open-circuit potential and (b) capacitance vs open-circuit potential.

Further investigations are presently carried out to unravel the detailed reasons for the favorable effect that GBA exerts on the performance of the DSC.

Transient photovoltage measurements were also performed for comparison. The recombination rate constant (k) of dye-sensitized cells is known to be dependent on the electrode potential. This effect was scrutinized, adjusting the V_{oc} by varying the intensity of the bias light. Figure 7a shows the logarithmic plot of k with respect to V_{oc}. The recombination rate constant, k, is apparently exponentially dependent on V_{oc}, and linear fits to all of the data give a similar slope value of 11.7 ± 0.3 for both cells, with or without of GBA coadsorption. This slope corresponds to ~90 mV per decade, which is slightly smaller than the value of 120 mV per decade obtained for solid-state cells.[30] Once again, the cell fabricated with a dye/GBA cografted TiO_2 film exhibits slower recombination at all potentials. However, the coadsorption does not influence the slope value, suggesting that the underlying recombination mechanism is not changed. It should be noted that the electron lifetimes obtained here (for example, at an open-circuit potential of -0.72V, 14 ms for device A and 24 ms for device B) are smaller than those observed by EIS measurements. This

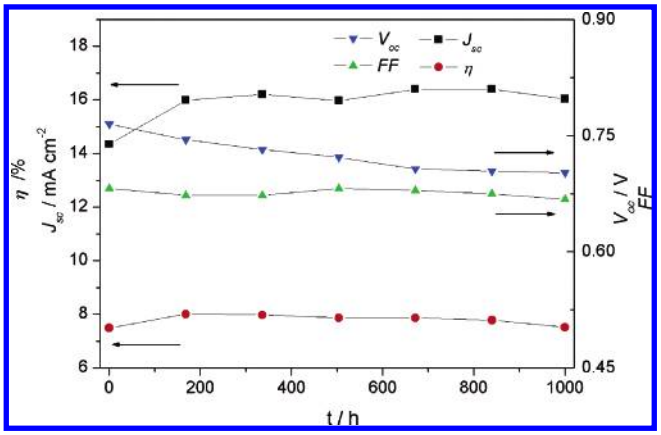

Figure 8. Detailed temporal evolution of photovoltaic parameters of device B under successive 1.0 sun visible-light soaking at 60 °C.

divergence should be attributed to the local concentration difference in electron-capturing species, I_3^-, due to the fact that the EIS was measured in the dark where the concentration of I_3^- is much less than that under illumination.[28]

As discussed in the analysis section, the capacitance can be calculated from the transient voltage data taken at each V_{oc}. The curve of capacitance vs open-circuit potential is shown in Figure 7b for two typical cells fabricated with TiO_2 film in the absence and the presence of GBA cografting. The curve is well fit by a single exponential, as has been found by other authors.[34,36,37] The cell with GBA coadsorption is found to have less capacitance at all potentials, which is in agreement with the EIS experiments.

Stability Test. Device B showed excellent light-soaking stability when subjected to the accelerated experimental conditions in the solar simulator at 60 °C covered by an ultraviolet-absorbing polymer film. Following 1000 h of light soaking under these conditions, there is no degradation in the device efficiency (Figure 8) as compared to the initial values. With nearly constant *FF* values (changes less than 2% were observed), the extraordinary stability is mainly due to the fact that the decrease in V_{oc} is well compensated by the increase in J_{sc}. At the end of the light soaking test, the J_{sc} was even larger than the initial value. These results also confirmed that the styryl structure in the K-19 sensitizer molecules can remain intact under the long-time visible light soaking as mentioned previously and, thus, paves the way for future designs of sensitizer with a high molar extinction coefficient exhibiting good thermostability.

Conclusions

The experiments disclosed in this study show that the coadsorption of K-19 sensitizer with 4-guanidinobutyric acid onto nanocrystalline TiO_2 films remarkably increases the photovoltage without suffering significant current penalty, thus, enhancing the total power conversion efficiency. Results from cyclic voltammetry, electrochemical impedance spectroscopy, and photovoltage transient measurements demonstrate that this increase in photovoltage is generated from the negative shift of the quasi-Fermi level of TiO_2 nanocrystals, as well as the inhibition of charge transfer from electrons in TiO_2 to the triiodide in the electrolyte primarily resulting from the shielding of surface traps due to the addition of GBA as a dye coadsorbent. The device showed a long-term stability exhibiting approximately 8% power conversion efficiency under the dual stress of both thermal aging and light soaking. Studies are now underway to optimize the chain length and the structure of this type of coadsorbent for further improvement of cell performance.

Acknowledgment. We are grateful to P. Comte and R. Charvet for the film fabrication, Dr. Carole K. Grätzel, Dr. Augstin McEvoy, and Dr. Qing Wang for helpful discussions, and T. Koyanagi (CCIC, Japan) for a free sample of the 400-nm-sized light scattering anatase particles. The Swiss Science Foundation, the Swiss Federal Office for Energy (OFEN), the European Office of U.S. Air Force under Contract No. F61775-00-C0003, and the Swiss Commission of Technology and Innovation (CTI) under contract no. 7019.1 NMS-NM have supported this work.

References and Notes

(1) O'Regan, B.; Grätzel, M. *Nature* **1991**, *353*, 737.
(2) Grätzel, M. *Nature* **2001**, *414*, 338.
(3) Hagfeld, A.; Grätzel, M. *Chem. Rev.* **1995**, *95*, 49.
(4) Grätzel, M. *J. Photochem. Photobiol., A* **2004**, *164*, 3.
(5) Grätzel, M. *Chem. Lett.* **2005**, *34*, 8.
(6) Wang, P.; Klein, C.; Humphry-Baker, R.; Zakeeruddin, S. M.; Grätzel, M. *Appl. Phys. Lett.* **2005**, *86*, 123508.
(7) Fischer, A. C.; Peter, L. M.; Ponomarev, E. A.; Walker, A. B.; Wijayantha, K. G. U. *J. Phys. Chem. B* **2000**, *104*, 949.
(8) Shkrob I. A.; Sauer, M. C. *J. Phys. Chem. B* **2004**, *108*, 12497.
(9) Tennakone, K.; Perera, V. P. S.; Kottegoda, I. R. M.; De Silva, L. A. A.; Kumara, G.; Konno, A. *J. Electron. Mater.* **2001**, *30*, 992.
(10) Gregg, B. A.; Pichot, F.; Ferrere, S.; Fields, C. L. *J. Phys. Chem. B* **2001**, *105*, 1422.
(11) Kumara, G.; Tennakone, K.; Perera, V. P. S.; Konno, A.; Kaneko, S.; Okuya, M. *J. Phys. D: Appl. Phys.* **2001**, *34*, 868.
(12) Zaban, A.; Chen, S. G.; Chappel, S.; Gregg, B. A. *Chem. Commun.* **2000**, 2231.
(13) Chappel, S.; Chen, S. G.; Zaban, A. *Langmuir* **2002**, *18*, 3336.
(14) Palomares, E.; Clifford, J. N.; Haque, S. A.; Lutz, T.; Durrant, J. R. *J. Am. Chem. Soc.* **2003**, *125*, 475.
(15) Wang, P.; Zakeeruddin, S. M.; Humphry-Baker, R.; Moser, J.-E.; Grätzel, M. *Adv. Mater.* **2003**, *15*, 2101.
(16) Wang, P.; Zakeeruddin, S. M.; Comte, P.; Charvet, R.; Humphry-Baker, R.; Grätzel, M. *J. Phys. Chem. B* **2003**, *107*, 14336.
(17) Wang, P.; Klein, C.; Humphry-Baker, R.; Zakeeruddin, S. M.; Grätzel, M. *J. Am. Chem. Soc.* **2005**, *127*, 808.
(18) Barbé, C. J.; Arendse, F.; Comte, P.; Jirousek, M.; Lenzmann, F.; Shklover, V.; Grätzel, M. *J. Am. Ceram.* Soc. **1997**, *80*, 3157.
(19) Kern, R.; Sastrawan, R.; Ferber, J.; Stangl, R.; Luther, J. *Electrochim. Acta* **2002**, *47*, 4213.
(20) Bisquert, J. *Phys. Chem. Chem. Phys.* **2003**, *5*, 5360.
(21) Hauch, A.; Georg, A. *Electrochim. Acta* **2001**, *46*, 3457.
(22) Zaban, A.; Meier, A.; Gregg, B. A. *J. Phys. Chem. B* **1997**, *101*, 7985.
(23) Schwarzburg, K.; Willig, F. *J. Phys. Chem. B* **2003**, *107*, 3552.
(24) Bisquert, J. *J. Phys. Chem. B* **2002**, *106*, 325.
(25) Fabregat-Santiago, F.; Garcia-Canadas, J.; Palomares, E.; Clifford, J. N.; Haque, S. A.; Durrant, J. R.; Garcia-Belmonte, G.; Bisquert, J. *J. Appl. Phys.* **2004**, *96*, 6903.
(26) Pitarch, A.; Garcia-Belmonte, G.; Mora-Sero, I.; Bisquert, J. *Phys. Chem. Chem. Phys.* **2004**, *6*, 2983.
(27) Fabregat-Santiago, F.; Bisquert, J.; Garcia-Belmonte, G.; Boschloo, G.; Hagfeldt, A. *Sol. Energy Mater. Sol. Cells* **2005**, *87*, 117.
(28) Wang, Q.; Moser, J.; Grätzel, M. *J. Phys. Chem. B* **2005**, *109*, 14945.
(29) O'Regan, B. C.; Lenzmann, F. *J. Phys. Chem. B* **2004**, *108*, 4342.
(30) O'Regan, B. C.; Scully, S.; Mayer, A. C.; Palomares, E.; Durrant, J. *J. Phys. Chem. B* **2005**, *109*, 4616.
(31) Moser, J.; Punchihewa, S.; Infelta, P. P.; Grätzel, M. *Langmuir* **1991**, *7*, 3012.
(32) Wang, Q.; Zakeeruddin, S. M.; Cremer, J.; Bäuerle, P.; Humphry-Baker, R.; Grätzel, M. *J. Am. Chem. Soc.* **2005**, *127*, 5706.
(33) Fabregat-Santiago, F.; Mora-Seró, I.; Garcia-Belmonte, G.; Bisquert, J. *J. Phys. Chem. B* **2003**, *107*, 758.
(34) Van de Lagemaat, J.; Park, N.-G.; Frank, A. J. *J. Phys. Chem. B* **2000**, *104*, 2044.
(35) Schlichthörl, G.; Huang, S. Y.; Sprague, J.; Frank, A. J. *J. Phys. Chem. B* **1997**, *101*, 8141.
(36) Willis, R. L.; Olson, C.; O'Regan, B.; Lutz, T.; Nelson, J.; Durrant, J. R. *J. Phys. Chem. B* **2002**, *106*, 7605.
(37) Duffy, N. W.; Peter, L. M.; Rajapakse, R. M. G.; Wijayantha, K. G. U. *Electrochem. Commun.* **2000**, *2*, 658.